Journal of Sound and Vibration 328 (2009) 301–317

Contents lists available at ScienceDirect

Journal of Sound and Vibration

journal homepage: www.elsevier.com/locate/jsvi

A parametric study on the dynamics of urban transit maglev vehicle running on flexible guideway bridges

Jun-Seok Lee [a], Soon-Duck Kwon [b,*], Moon-Young Kim [a], In Ho Yeo [c]

[a] Department of Civil and Environmental Engineering, Sungkyunkwan University, Cheoncheon, Jangan, Suwon 440-746, South Korea
[b] Department of Civil Engineering, Chonbuk National University, Chonju, Chonbuk 561-756, South Korea
[c] Railroad Structure Research Department, Korea Railroad Research Institute, Uiwang, Kyoungki 437-757, South Korea

ARTICLE INFO

Article history:
Received 9 March 2009
Received in revised form
19 July 2009
Accepted 11 August 2009
Handling Editor: J. Lam
Available online 2 September 2009

ABSTRACT

The purpose of this study is to develop a numerical model for a dynamic interaction analysis of an actively controlled maglev vehicle and flexible guideway structure. In addition, an investigation is performed of the effect of vehicle and guideway characteristics on dynamic responses of low and medium speed maglev systems. Dynamic governing equations are derived by combining the 5-dof maglev vehicle model, the modal properties of guideway structures and a LQG controller for electromagnetic suspension. An investigation is then carried out on the effect of vehicle models, vehicle speed, irregularity, guideway deflection ratio, span length, span continuity and damping ratio on dynamic responses of the relatively low speed maglev vehicle and guideway structures. From the numerical simulation, it is found that the air gap of the vehicle is strongly affected by vehicle speed, tract roughness and guideway deflection ratio. In particular, the guideway deflection ratio is the most influential parameter which governs the air gap. Continuous span girders are found to be effective in reducing the air gap because of its smooth curvature and small deflection slope near the support. However, the span length and damping ratio of the guideway structure do not affect the air gap. The overall dynamic magnification factor of the guideway girder is not severe compared to the traditional wheel type vehicle.

1. Introduction

Non-contact magnetically levitated (maglev) vehicles with linear motor propulsion have been studied since the 1970s [1,2]. The advantages of the maglev system compared with the conventional wheel-rail system are known to be its reduced risk of derailment, increased riding comfort, reduced noise, reduced need for maintenance of the guideway, and energy saving [3].

High speed maglev systems have been developed mostly in Germany and Japan where running test lines have been constructed. These studies have essentially focused on the speed and technology required for inter-city transportation, and have resulted in the operation of the first commercial line in Shanghai, China. However, high speed ground transportation in most countries is already occupied by wheel type railway systems such as TGV, ICE and Shinkansen. Therefore, use of the high speed maglev system is not widespread, with the exception of the new line at Shanghai. Although plans for commercial maglev lines exist in several countries, their realization and the future of high speed maglev systems is not yet clear.

* Corresponding author. Tel.: +82 63 270 2289; fax: +82 63 270 2421.
E-mail address: sdkwon@chonbuk.ac.kr (S.-D. Kwon).

0022-460X/$ - see front matter © 2009 Elsevier Ltd. All rights reserved.
doi:10.1016/j.jsv.2009.08.010

Nomenclature

a_j	distance from cabin center to jth bogie
A	effective areas of magnetic pole
c_s	damping of secondary suspension
E_{deflec}	energy caused by guideway deflection
E_D	dissipation energy caused by viscous damping of the secondary suspension
E_K	kinetic energy of bogie mass
E_M	linearized electromagnetic energy of the primary suspension
E_{rough}	energy caused by surface roughness
E_S	elastic strain energy of spring at the secondary suspension
F_m	magnetic force
i	current in the circuit
i_0	current at static equilibrium
I_c	mass moments of inertia about pitch motion of cabin
k_s	stiffness of secondary suspension
k_i	equivalent stiffness proportion to current
k_z	equivalent stiffness proportion to derivative of air gap
m_b	mass of each bogie
m_c	mass of cabin
L_0	inductance of magnet winding at static equilibrium
n	number of concerned guideway modes
N	number of turn of coil
q	generalized coordinate of guideway
R	reluctance
V	vehicle speed
z_0	air gap at static equilibrium
z_b	vertical displacement of bogie
z_{bg}	air gap between bogie and guideway
Δz_{bg}	air gap fluctuation at nominal state
z_c	vertical displacement of cabin
z_{c0}	initial displacement of spring at secondary suspension
z_{cb}	relative displacement between cabin and bogie
z_g	vertical displacements of guideway
z_r	track roughness

Matrix and vector

$\mathbf{A}$	state matrix
$\mathbf{B}$	location matrix of controller
$\mathbf{C}$	measurement matrix of state
$\mathbf{D}$	measurement matrix of controller
$\mathbf{f}$	sensor noise vector
$\mathbf{G}$	state feedback gain matrix
$\mathbf{H}$	location matrix of excitation
$\mathbf{L}$	observer gain matrix
$\mathbf{u}$	control force vector
$\mathbf{w}$	external excitation vector
$\mathbf{x}$	state vector
$\hat{\mathbf{x}}$	state estimator
$\mathbf{y}$	output vector

Greek letters

θ_c	pitch angle of cabin
μ_0	magnetic permeability of vacuum
ξ	damping ratio of guideway
ϕ	mode shape of guideway
ω	natural frequency(rad/s) of guideway

In order to promote maglev technology, the urban transit maglev system is currently being developed in Korea to provide effective transportation in metropolitan areas as an alternative to the low and medium speed transportation system dominated by light rail, rapid transit and commuter rail. Thus the nominal operating speed of the urban transit maglev ranges from 0 to 100 km/h. In Korea, the UTM (urban transit maglev) system has been in development since the end of the 1980s, giving rise to the successful operation of the first version of the system [4–6], UTM-01, in a short test line (see Fig. 1).

Although the maglev is regarded as a future transportation system, very limited research has been performed in the field of the maglev vehicle–guideway structure interaction problem. Hedrick et al. [7] carried out a numerical simulation for a simple maglev vehicle running on a two-span continuous guideway bridge in order to investigate vehicle riding quality. Cai et al. [8] performed a parametric study on short span bridges crossed by a 2-dof maglev vehicle with passive spring and dashpot suspension. Recently, Kwon et al. [9] performed a numerical simulation for an 11-dof maglev vehicle with equivalent passive suspension running on a suspension bridge under gusty winds in order to test the applicability of such a flexible bridge for the guideway structure.

Concerning the German Maglev Transrapid, Popp and Schiehlen [10] derived the formulation for the vehicle–guideway dynamics including feedback control. Zhao and Zhai [11] investigated the ride quality of a two-dimensional model of the German Transrapid maglev vehicle with an equivalent passive suspension running on a simple beam. Meisinger [12] performed the numerical simulation for a single mass maglev vehicle on an elastic single and double-span guideway moving with both constant magnet force and constant magnet gap. Hägele and Dignath [13] recently studied a simulation of the transfer of a Transrapid vehicle over several guideway girders using the control law for the magnet forces which is simplified by the characteristics of linear spring–damper elements.

Tsunashima and Abe [14] constructed a dynamic model for an active magnetic suspension and compared results with field tests. Zheng et al. [15] performed a numerical simulation of a coupled 5-dof maglev vehicle and guideway system with a controllable feedback magnetic force. Fang et al. [16] studied dynamic modeling and control of the Magplane vehicle. Morita et al. [17] investigated the environmental influence on levitation control from the field test of the Linimo Line (HSST

Fig. 1. Urban transit maglev vehicle in test track.

system) during EXPO2005. Han et al. [6] performed a finite element based numerical simulation of the Korean UTM-01 maglev vehicle and guideway structures by using a large number of elements.

Previous studies focused either on the stability of the magnetic force or on control efficiency, while minimal interest has been paid to the dynamic characteristics of the guideway system and its effects on the maglev vehicle and guideway interaction system. Considering that 40–80 percent of the initial costs are likely to be invested in the construction of the guideway bridges [3,8], more emphasis should be placed on research into the guideway system itself.

In this paper, a theoretical model for active controlled maglev vehicles and guideway structures is presented to investigate the dynamic behaviors of the maglev-guideway coupling system. A 5-dof maglev vehicle model is developed from the method used in conventional vehicle dynamics [18,19]. The governing equation of motion is derived by combining the maglev vehicle model, the modal properties of guideway structures and the active controller for electromagnetic suspension. From the numerical simulations for UTM-01, which is a low and medium speed maglev system for urban transportation, the air gap fluctuation of the maglev vehicle and dynamic amplification factor of the guideway are mainly examined based on various parameters such as vehicle models, vehicle speed, irregularity, guideway deflection ratio, span length, span continuity, and damping ratio of the guideway.

2. Governing equations

2.1. Electromagnetic force

The suspension force is derived from the force attraction between the electromagnetic and ferromagnetic objects. The electromagnetic force acting on a track at any instant of time is expressed as [1]

$$F_m(t) = \mu_0 A \left(\frac{Ni(t)}{2z_{\mathrm{bg}}(t)} \right)^2 \tag{1}$$

where μ_0 is the magnetic permeability of the vacuum, A is the effective areas of the magnetic pole, N is the number of turns of coil, $i(t)$ is the current in the circuit, and z_{bg} is the air gap between the magnet and reaction plate of the guideway.

The linearized electromagnetic model at the nominal equilibrium point is used in the present study. For linearization of the magnetic force, the air gap at any instant of time, can be divided into a nominal component at static equilibrium z_0, and the small fluctuating component Δz_{bg}. The corresponding current is also divided into i_0 and Δi. By substituting these relationships into Eq. (1), the linearized magnetic force can then be obtained as follows [1]:

$$F_m(t) = F_{m0} + k_i \Delta i(t) - k_z \Delta z_{\mathrm{bg}}(t) \tag{2}$$

where F_{m0} is the magnetic force at the nominal static equilibrium point, and k_i and k_z are the equivalent stiffness which are dependent on current and derivative of air gap, respectively,

$$F_{m0} = \frac{\mu_0 N^2 A}{4} \left(\frac{i_0}{z_0} \right)^2 \tag{3a}$$

$$k_i = \frac{\mu_0 N^2 A i_0}{2 z_0^2} \tag{3b}$$

$$k_z = \frac{\mu_0 N^2 A i_0^2}{2 z_0^3} \tag{3c}$$

The relationship between the current rate, current and voltage can be written as the following first order differential equation in terms of reluctance R_0, and the inductance of magnet winding at equilibrium point, L_0:

$$\Delta\dot{i}(t) = \frac{k_z}{k_i}\Delta\dot{z}_{bg}(t) - \frac{R_0}{L_0}\Delta i(t) + \frac{1}{L}\Delta v(t) \tag{4}$$

2.2. Guideway structures

Guideway structures mostly consist of reaction plates, sleepers, girder, and piers (see Fig. 4). The magnetic forces of the vehicle are transmitted from the bogies to the reaction plate, and then to the pier through the girder. While the mechanism of the force transmission from car to bridge is slightly more complicated than in an ordinary vehicle–bridge system, it is reasonable to assume that there is no relative deflection between the reaction plate and girder. This means that the magnetic forces are directly transmitted to the girder.

The pier is generally assumed to be a rigid base for a short span guideway system. The flexural stiffness of reaction plates and sleepers is negligible compared to the girder. Consequently, the guideway structure can be regarded as a lateral beam on supports. The girder is modeled using commercial structural analysis software, the ABAQUS, based on the finite element method.

Because the number of degrees of freedom of the girder is generally much larger than that of the maglev vehicle, reducing the number of equations by applying the mode superposition method to the girder appears reasonable for computational efficiency. By applying the expansion theorem, the displacements of the girder can be expressed as a summation of each component of the normalized mode shape $\phi(x)$ and generalized coordinate $q(t)$:

$$z_g(x,t) = \sum_l \phi_l(x) q_l(t) \tag{5}$$

The equation of motion for the guideway girder can be expressed as follows [9]:

$$\ddot{q}_l(t) + 2\xi_l\omega_l\dot{q}_l(t) + \omega_l^2 q_l(t) = \phi_l(x) F_m(t) \tag{6}$$

where ξ and ω are the damping ratio and natural frequency of lth mode of a guideway girder, respectively, and F_m is the magnetic force given from the vehicle to the guideway.

2.3. Coupled motion for maglev vehicle and guideway structures

The dynamic model for the idealized 5-dof maglev vehicle shown in Fig. 2 consists of one cabin and three bogies. From the force equilibrium, the linearized equation of motion for a car cabin and three bogies can be obtained as follows:

$$\ddot{z}_c(t) = -\sum_{j=1}^{3}\left\{\frac{k_s}{m_c}(z_c(t) - a_j\theta_c(t) - z_{bj}(t)) + \frac{c_s}{m_c}(\dot{z}_c(t) - a_j\dot{\theta}_c(t) - \dot{z}_{bj}(t))\right\} \tag{7a}$$

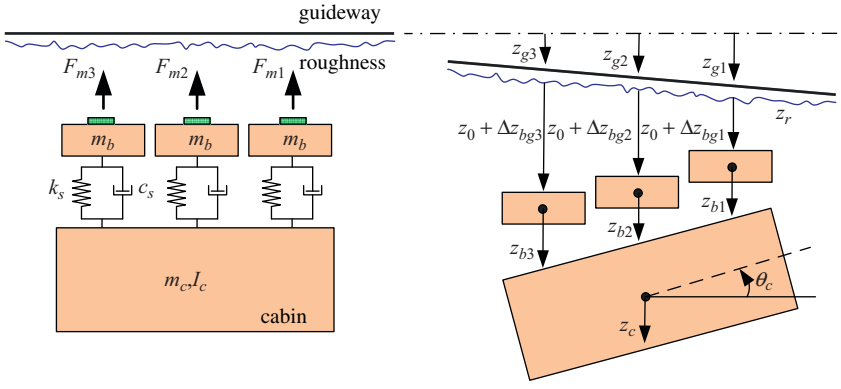

Fig. 2. Dynamic model for 5-dof maglev vehicle and guideway girder.

$$\ddot{\theta}_c(t) = \sum_{j=1}^{3} a_j \left\{ \frac{k_s}{I_c}(z_c(t) - a_j\theta_c(t) - z_{bj}(t)) + \frac{c_s}{I_c}(\dot{z}_c(t) - a_j\dot{\theta}_c(t) - \dot{z}_{bj}(t)) \right\} \tag{7b}$$

$$\ddot{z}_{bj}(t) = \frac{k_s}{m_b}(z_c(t) - a_j\theta_c(t) - z_{bj}(t)) + \frac{c_s}{m_b}(\dot{z}_c(t) - a_j\dot{\theta}_c(t) - \dot{z}_{bj}(t)) - \frac{k_i}{m_b}\Delta i_j(t) + \frac{k_z}{m_b}\Delta z_{\mathrm{bg}j}(t), \quad j = 1,2,3 \tag{7c}$$

where z_c is the vertical displacement of the cabin, $_c$ is the pitch angle of the cabin, z_{bj} is the vertical displacement of the jth bogie, $z_{\mathrm{bg}j}$ is the air gap between the jth bogie and the guideway structure, a_j is the distance from the cabin center to the jth bogie, m_c is the mass of the cabin, m_b is the mass of each bogie, I_c is the mass moments of inertia about the pitch motion of the cabin, k_s is the stiffness of secondary suspension, c_s is the damping of secondary suspension, and subscript-j represents the jth bogie. The relative displacement between the cabin and the jth bogie can be expressed by

$$z_{\mathrm{cb}j}(t) = z_c(t) - a_j\theta_c(t) - z_{bj}(t) \tag{8}$$

By applying the expansion theorem in Eq. (5), the relative air gap between the jth bogie and the guideway structure can be given by the following equation:

$$\Delta z_{\mathrm{bg}j}(t) = z_{bj}(t) - \sum_{l=1}^{n} \phi_l(x_j)q_l(t) - z_r(x_j) - z_0 \tag{9}$$

where $x_j = x_c - a_j$, z_0 is air gap at static equilibrium, and x_c is the position of the car cabin at a instant time. In addition to the above equation, the differential equation for the current rate, current and voltage listed in Eq. (4) should be applied for each bogie, respectively. Substituting Eqs. (8) and (9) into Eq. (7), and combining it with Eqs. (4) and (6), the following equation of motion can finally be derived:

$$\dot{\mathbf{x}}(t) = \mathbf{A}\mathbf{x}(t) + \mathbf{B}\mathbf{u}(t) + \mathbf{H}\mathbf{w}(t) \tag{10}$$

where $\mathbf{x} = [q_1 \cdots q_n, \dot{q}_1 \cdots \dot{q}_n, z_c, \theta_c, \Delta z_{\mathrm{bg}1}, \Delta z_{\mathrm{bg}2}, \Delta z_{\mathrm{bg}3}, \dot{z}_c, \dot{\theta}_c, \Delta\dot{z}_{\mathrm{bg}1}, \Delta\dot{z}_{\mathrm{bg}2}, \Delta\dot{z}_{\mathrm{bg}3}, \Delta i_1, \Delta i_2, \Delta i_3]^{\mathrm{T}}$ is the state vector, $\mathbf{A}$ is the state matrix, $\mathbf{B}$ is the location matrix of the controller, $\mathbf{H}$ is the location matrix of excitation, $\mathbf{w}$ is the external excitation vector, and $\mathbf{u}$ is the control force vector. The MATHEMATICA, a commercial scientific software, was used to derive the equation of motion and sub-matrices that are given in Appendix A.

3. Dynamic simulations

3.1. Control algorithm

Since the magnetic forces produced by a constant electromagnetic current are approximately inverse proportional to the air gap, the ferromagnetic suspension system is inherently unstable. Consequently, a means of active control needs to be incorporated for stable suspension [1]. The choice of an appropriate control algorithm among the several modern control methods is dependent on the objective of control, availability of measurements for feedback, and the nature of external disturbances.

It is generally not possible to directly measure all state variables because of cost or inaccessibility. Some selected output variables which depend on the state variables are measured in practice. Therefore, an observer is inevitably required for state estimation. In the present study, a LQG (Linear Quadratic Gaussian) controller is designed by combining the Kalman estimator with a linear quadratic regulator [20,21]. It should be noted that the LQG controller is not an actual control algorithm for UTM-01, but is used for comparative study.

In the design of the observer that estimates state variables with a minimal mean square estimation error among all estimates, uncorrelated external disturbance $w(t)$ and sensor noise $f(t)$ are assumed to be Gaussian white noise processes. The state estimator is expressed as follows [20]:

$$\dot{\hat{\mathbf{x}}}(t) = \mathbf{A}\hat{\mathbf{x}}(t) + \mathbf{B}\mathbf{u}(t) + \mathbf{L}(\mathbf{y}(t) - \mathbf{C}\hat{\mathbf{x}}(t)) \tag{11}$$

where $\mathbf{L}$ is the observer gain matrix, and is obtained by solving the Riccati equation. In order to model the maglev system, the following output equation is used in conjunction with the equation of motion described in Eq. (10):

$$\mathbf{y}(t) = \mathbf{C}\mathbf{x}(t) + \mathbf{D}\mathbf{u}(t) + \mathbf{f}(t) \tag{12}$$

where $\mathbf{y}(= [\Delta z_{\mathrm{bg}1}\ \Delta\dot{z}_{\mathrm{bg}1}\ \Delta z_{\mathrm{bg}2}\ \Delta\dot{z}_{\mathrm{bg}2}\ \Delta z_{\mathrm{bg}3}\ \Delta\dot{z}_{\mathrm{bg}3}]^{\mathrm{T}})$ is the output vector, and consists of the air gap and its velocity at each bogie in this study. In addition, $\mathbf{C}$ is the measurement matrix of state, $\mathbf{D}$ is the measurement matrix of the controller, and $\mathbf{f}$ is the sensor noise vector. Multiplying the state feedback gain matrix ($\mathbf{G}$) by the state estimate vector, the control voltage can be given by the following equation. The state feedback gain can be evaluated from the linear quadratic regulator:

$$\mathbf{u}(t) = \Delta v(t) = -\mathbf{G}\hat{\mathbf{x}}(t) \tag{13}$$

Final governing equations for the interaction system between the maglev vehicle, the guideway structure and the controller can be obtained in the following form:

$$\begin{Bmatrix} \dot{\mathbf{x}}(t) \\ \dot{\hat{\mathbf{x}}}(t) \end{Bmatrix} = \begin{bmatrix} \mathbf{A} & -\mathbf{BG} \\ \mathbf{LC} & \mathbf{E} \end{bmatrix} \begin{Bmatrix} \mathbf{x}(t) \\ \hat{\mathbf{x}}(t) \end{Bmatrix} + \begin{bmatrix} \mathbf{H} & \mathbf{0} \\ \mathbf{0} & \mathbf{L} \end{bmatrix} \begin{Bmatrix} \mathbf{w}(t) \\ \mathbf{f}(t) \end{Bmatrix} \tag{14}$$

where $\mathbf{E} = \mathbf{A} - \mathbf{BG} - \mathbf{LC}$. Detail sub-matrices are provided in Appendix B. The above ordinary differential equation can be solved numerically by the Runge–Kutta Method [22].

3.2. Energy formulation for bogies

The equation of motion is focused on the determination of displacements, velocities, and forces. However, the energy for each parameter is generally suitable for comparison of relative contribution to the system responses. An energy representation can be formed by integrating the individual forces in Eq. (7c) over entire displacement history [23]. The resulting energy for bogie of the maglev vehicle becomes as follows:

$$E_K + E_S = E_C + E_M - E_D \tag{15}$$

where E_K is the kinetic energy of bogie mass, E_S is the elastic strain energy of spring at the secondary suspension, E_C is the energy fed to the system via the cabin motion, E_M is the energy fed to the system via the electromagnetic primary suspension, E_D is the dissipation energy caused by viscous damping of the secondary suspension. The individual energies of Eq. (15) are given in Appendix C.

Considering the free body diagram of the bogies shown in Fig. 2, the source of input energy to the system is the electromagnetic primary suspension and the cabin motion. The only output of energy is viscous damping at the secondary suspension. Therefore, the internal energy within the system border on the left-hand side of Eq. (15) stay constant in the long run, and balance with external energy which includes the input and output energy on the right-hand side of Eq. (15).

3.3. Irregularity of guideway

The reaction plates on the guideway girder directly support the electromagnetic forces given by the maglev vehicle, and transmit these to the girder. The irregularity of the reaction plates that corresponds to the rail in a conventional railway is one of the main sources that produce vibrations of the vehicle and guideway structures. The geometry of the reaction plates is defined in terms of four irregularities consisting of gage, cross level, alignment, and vertical surface profile [18]. Among them, the gage, cross level, and alignment have generally insignificant effects on the quality control of guideway structures made of precast and prefabricated members. Therefore, the sole vertical surface irregularity of the rail is considered in this study.

The vertical surface irregularity is generally expressed as a power spectral density (PSD) function. There are many types of PSD functions for various surface transportation systems [1,18,24]. Although the PSD function proposed by Tsunashima and Abe [14] has been used by some researchers for the maglev system [11,15], it was not derived based on field measurement.

In this study, the actual roughness of the maglev guideway is used for simulation. Fig. 3 shows irregularity profiles of reaction plates that were measured at the test tract in the Korean Institute of Machinery and Materials, as shown in Fig. 1 [25]. The roughness profiles were measured at every 1.25 m along the test tract based on the versine technique [17].

Three types of roughness profile are used for simulation. The first type is a normal condition based on the measured profile data which has a maximum irregularity ranging around ± 4.1 mm. The second and third types are fair and poor conditions, respectively, with maximums of ± 2.1 and ± 6.1 mm, respectively. The fair and poor conditions are only given for comparative studies by changing the amplitude scale of the normal condition, and are not an experimental data.

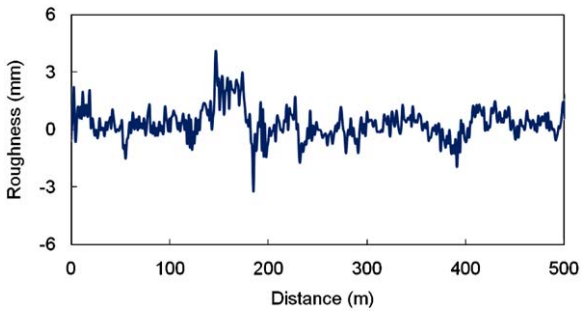

Fig. 3. Measured vertical roughness profile of the test tract at Korean Institute of Machinery and Materials [25].

3.4. Vehicle and guideway structures

A numerical example for the maglev vehicle and guideway structure is given here in order to quantitatively simulate the coupling behaviors. The vehicle used in the present study is basically that used for the UTM-01 [4,25] which is very similar to the car shown in Fig. 1, and the properties are given in Table 1. The maglev system basically consists of two cars in ordinary operation. The nominal air gap of the UTM-01 is 10 mm.

Fig. 4 shows a concept drawing for the guideway structure currently under development [26]. The guideway structures are intended to consist of a prestressed concrete box girder with a single span, two continuous spans and three continuous

Table 1
Properties of the UTM-01 maglev vehicle [4,25].

Parameter	Value
Mass of car Body (m_c)	
Empty	12.1 t
Normally loaded	15.5 t
Fully loaded	20.0 t
Mass moment of inertia (I_c)	242.2 t m
Mass of bogie (m_b)	3.1 t
Distance from cabin center to 1st bogie (a_1)	3.6 m
Distance from cabin center to 2nd bogie(a_2)	0 m
Distance from cabin center to 3rd bogie(a_3)	−3.6 m
Secondary suspension	
Stiffness (k_s)	150.6kN m^{-1}
Damping (c_s)	18.76kN s m^{-1}
Magnet	
Total resistance of circuit	12.8 Ω
Number of turned coil (N)	660
Area of magnet (A)	0.32 m^2
Current at nominal equilibrium point	20 A
Nominal air gap	10 mm

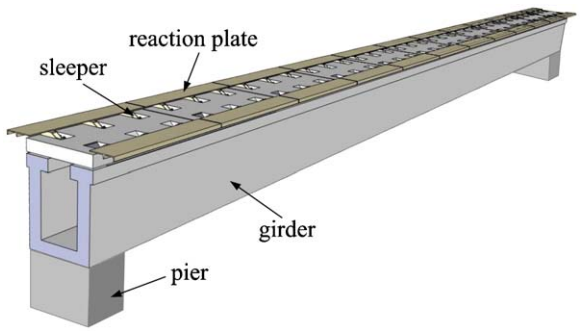

Fig. 4. Guideway structure [26].

Table 2
Structural properties of guideway girder.

Span length (m)	Deflection ratio	Maximum displacement (mm)	Width (m)	Height (m)	Thickness (m)	Area (m^2)	Mass moment of inertia (m^4)	Mass per unit length (ton m^{-1})	First natural frequency (Hz)
25	500	50.0	1.35	0.93	0.2	0.75	0.078	2.25	2.56
25	1000	25.0	1.35	1.21	0.2	0.86	0.157	2.59	3.38
25	1500	16.7	1.35	1.41	0.2	0.95	0.235	2.84	3.95
25	2000	12.5	1.35	1.58	0.2	1.01	0.314	3.04	4.41
25	2500	10.0	1.35	1.72	0.2	1.07	0.392	3.21	4.80
25	3000	8.3	1.35	1.85	0.2	1.12	0.471	3.36	5.13
20	1500	13.3	1.35	1.19	0.2	0.86	0.151	2.57	5.19
25	1500	16.7	1.35	1.41	0.2	0.95	0.235	2.84	3.95
30	1500	20.0	1.35	1.63	0.2	1.03	0.339	3.09	3.15
35	1500	23.3	1.35	1.83	0.2	1.11	0.461	3.34	2.60
40	1500	26.7	1.35	2.03	0.2	1.19	0.602	3.58	2.20

spans. Each span length is basically 25 m. By adjusting the stiffness and corresponding mass of the guideway, the ratio between one span length and maximum static deflection ranges from 500 to 5000 for parameter studies. The properties of the guideway structures are given in Table 2.

4. Parametric studies

Case studies are performed in order to understand the dynamic behaviors of the coupled system derived in the previous sections. The effects of various parameters of the maglev vehicle and guideway on the dynamic responses of the system are investigated. The analyses are performed mostly for a case whereby the maglev system consists of two cars that move on single span guideway girders with a span length of 25 m for each girder and a deflection ratio of 1500 at a normal roughness condition.

Fig. 5 shows time history responses of the maglev vehicle and guideway girder at a vehicle speed 110 km/h. To give an initial disturbance to the maglev vehicle before entering the guideway girder, the vehicle is excited a few second by the prescribed roughness corresponding to guideway deflection and surface roughness. As can be seen in the figure, the air gap fluctuation of each bogie peaks when the bogie cross from one span to the next span. This is because of the sharp slope and

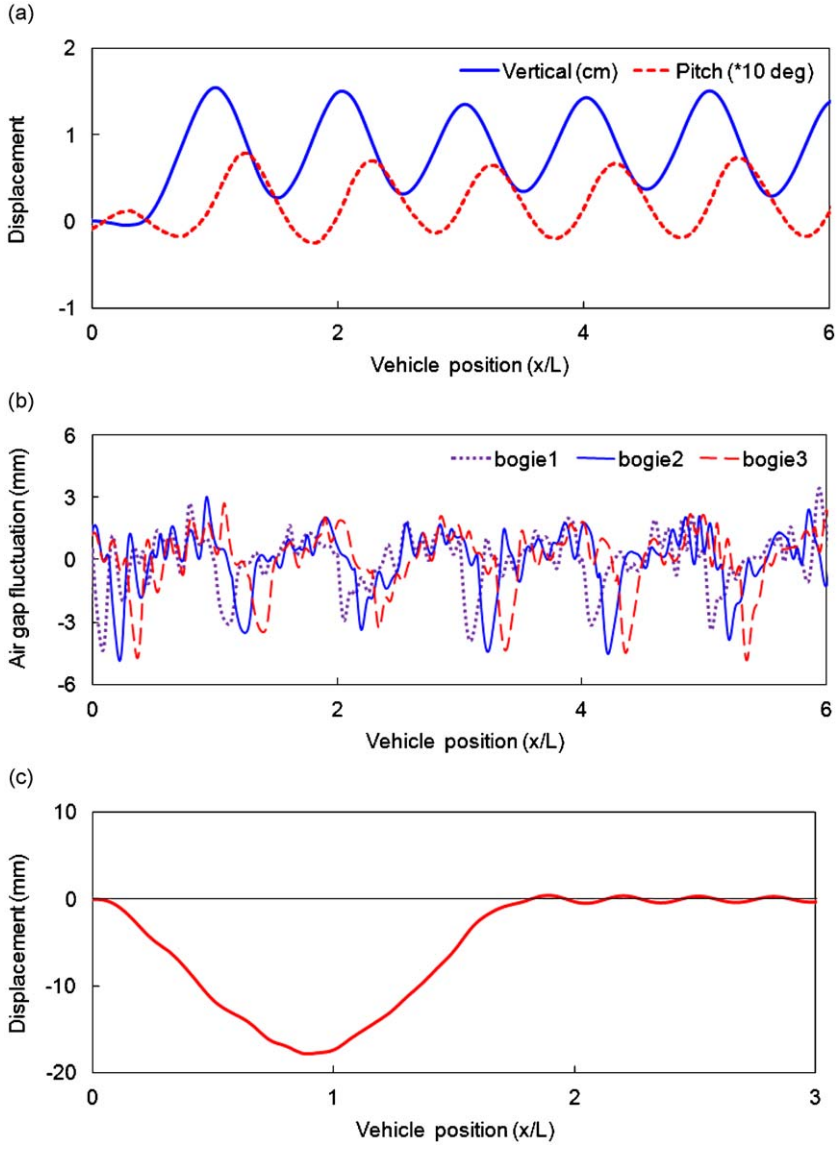

Fig. 5. Dynamic responses of maglev vehicle and guideway girder at $v = 110$ km/h: (a) vertical and pitching displacement of cabin; (b) air gap fluctuations of bogies at first car; and (c) guideway displacement at center of span.

abrupt change of the guideway deflection at the support. The displacement of the guideway girder seems to be close to the static influence line, even though the dynamic moving loads are applied to the girder.

4.1. Vehicle speed

Fig. 6 shows the air gap fluctuation of the maglev vehicle according to three different support conditions and various vehicle speeds. In the figure, "deflection" represents the case where the vehicle runs on a flexible guideway girder without surface roughness, and "roughness" indicates the case where the vehicle runs on irregular firm ground without deflection due to its weight.

It is clear from the figure that the air gap fluctuation is dominated by surface roughness at a low vehicle speed of <60 km/h, yet the deflection of the guideway girder gradually governs the air gap fluctuation at a high vehicle speed. As the vehicle speed increases, the responses of the vehicle are strongly affected by a long wave roughness which corresponds to the girder deflection.

The air gap fluctuation of the vehicle and the DMF (dynamic magnification factor) of the guideway girder for three different levels of roughness are shown in Fig. 7. As can be seen in the figure, the air gap fluctuation linearly increases in proportion to the vehicle speed. The DMF of the guideway girder caused by the maglev vehicle is generally not severe compared with that caused by a traditional railway load, and is not significantly affected by vehicle speed.

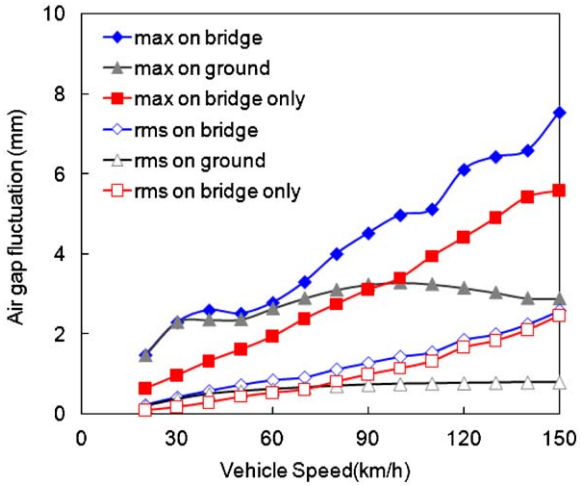

Fig. 6. Maximum air gap fluctuations of maglev vehicle running on various support conditions (deflection ratio = 1500, normal roughness).

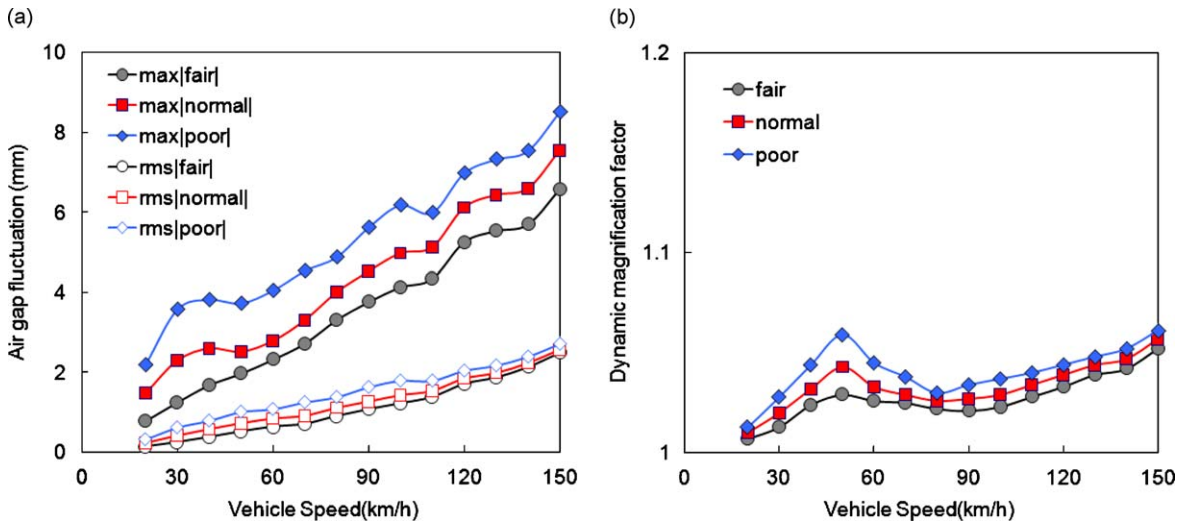

Fig. 7. Effect of roughness and vehicle speeds on dynamic responses (deflection ratio = 1500): (a) maximum air gap fluctuations of maglev vehicle for three different types of roughness and (b) dynamic magnification factor of guideway girder.

Two kinds of resonance vehicle speeds are generally used to check the amplification of response. The first is caused by vehicle passing and defined as fundamental bending frequency of girder multiplying by span length of girder. The second is induced by periodic hitting of bogies on girder and defined as fundamental bending frequency of girder multiplying by bogie distance. In this example guideway girder, the first and the second resonance vehicle speed are 355.5 and 51.2 km/h, respectively. The small hump of response around 50 km/h in Fig. 7(b) can be clearly explained as resonance phenomena caused by periodic excitation of bogies.

4.2. Roughness profile

Comparing the responses at the three different support conditions shown in Fig. 6, the exciting source of the air gap fluctuation at the bogies is clearly identified. The air gap fluctuation is mostly dominated by surface roughness at a low vehicle speed and by guideway deflection at a high vehicle speed. This implies that proper control of guideway deflection is necessary to increase the vehicle speed. The air gap is not affected by vehicle speed when the vehicle runs on firm ground.

Fig. 7(a) shows the air gap fluctuation of the maglev vehicle for three different levels of roughness. It can be clearly seen that the maximum amplitude of the air gap fluctuation is in proportion to that of roughness. However, the overall DMF of the guideway girder maintains a very low value, although there are slight differences depending on the roughness level.

4.3. Guideway deflection

Fig. 8 shows the air gap fluctuation and DMF of the guideway according to the guideway deflection ratio between span length and maximum static deflection amplitude when a vehicle runs on a flexible guideway. The deflection ratio of the guideway strongly affects the air gap fluctuation because the guideway deflection is a type of roughness with a very long wave length. The effects of the deflection ratio on the DMF of the guideway structure are negligible.

The nominal operation speed of the UTM-01 is restricted within 110 km/h, and the maximum allowable air gap fluctuation between the magnet at the bogie and the reaction plate at the guideway is ± 4 mm. Applying these constraints to Fig. 8(a), the criterion for guideway deflection can be obtained as 2000, which can be used to inversely determine the corresponding flexural stiffness of the girder. The criterion acquired from Fig. 8(a) is not generalized, and can be changeable depending on the control algorithm and dynamic properties of the vehicle and guideway structure.

4.4. Span length

Fig. 9 shows a comparison between the air gap fluctuation and DMF for three different span lengths of the guideway girder. Both the air gap and the DMF of the guideway are unaffected by span lengths. The DMF for various span lengths does not exceed 1.1. From the analysis results, it is found that the effects of the guideway span length on the dynamic responses of the vehicle and the guideway girder are insignificant.

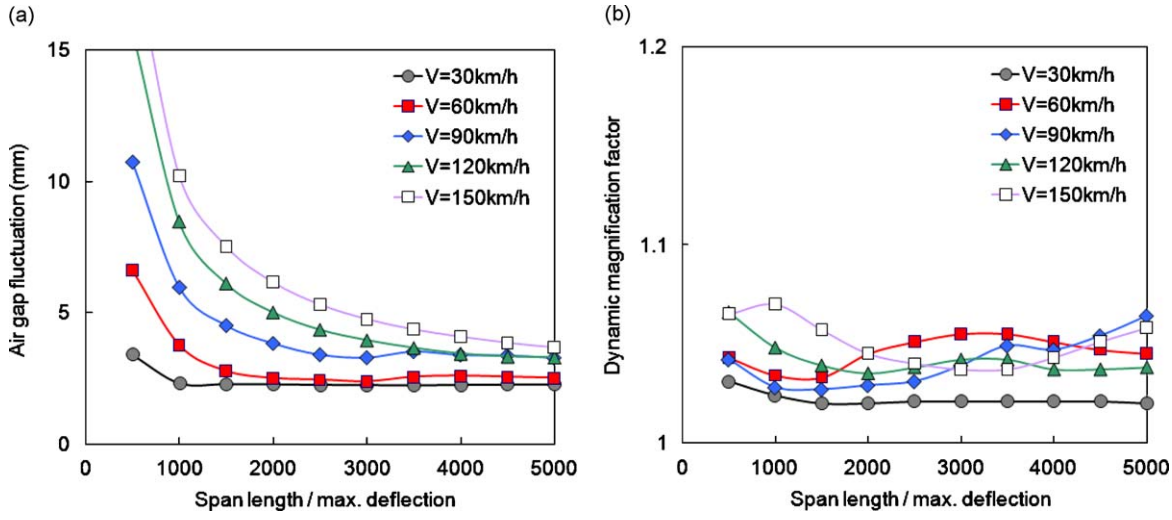

Fig. 8. Effect of deflection ratio between span length and maximum displacement of guideway with normal roughness: (a) maximum air gap fluctuations of maglev vehicle and (b) dynamic magnification factor of guideway girder.

4.5. Span continuity

The effect of span continuity on the air gap fluctuation and DMF are investigated for three different types of continuous guideway girders: the simply supported type, the two span continuous type, and the three span continuous type. As can be seen in Fig. 10, the span continuity does not affect the air gap at a low velocity, yet there are a number of discrepancies with the air gap depending on span continuity at a high vehicle speed in which guideway deflection dominates the air gap. The air gap fluctuation of a vehicle running on a three span continuous guideway girder is the smallest among the three, followed by that on the two span continuous girder. The effects of span continuity on the DMF of the guideway girder are negligible.

As can be seen in Fig. 5(b), the air gap fluctuation reaches a peak when the bogies pass through the support of the guideway girder. The continuous span girder has a relatively smooth curvature and a small deflection slope at its support compared with the simple span girder. These advantages of a continuous span girder attenuate the peaks of the air gap near the support and decrease the overall air gap of the vehicle.

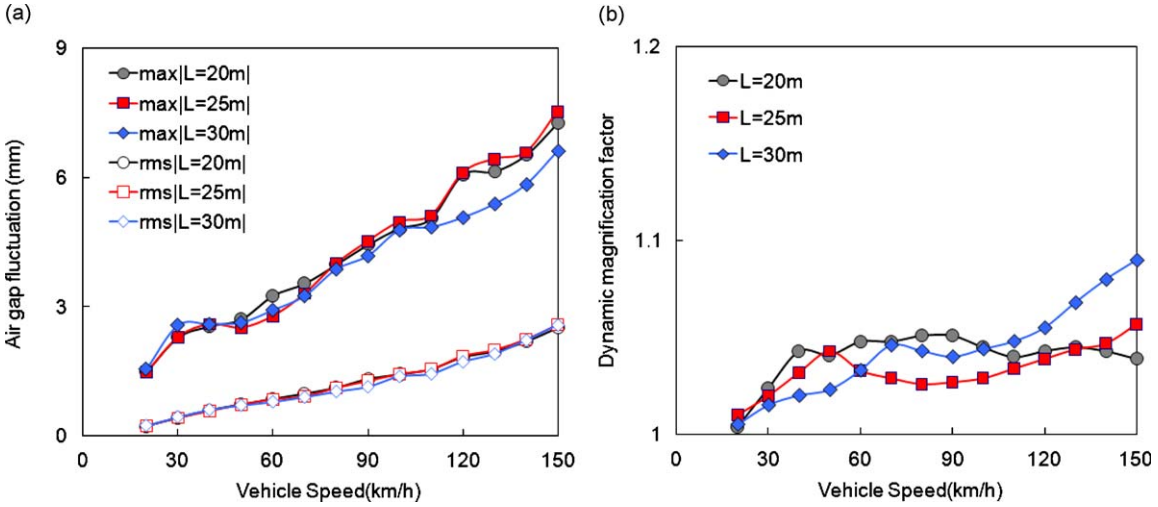

Fig. 9. Effect of span length on dynamic responses (deflection ratio = 1500, normal roughness): (a) maximum air gap fluctuations of maglev vehicle and (b) dynamic magnification factor of guideway girder.

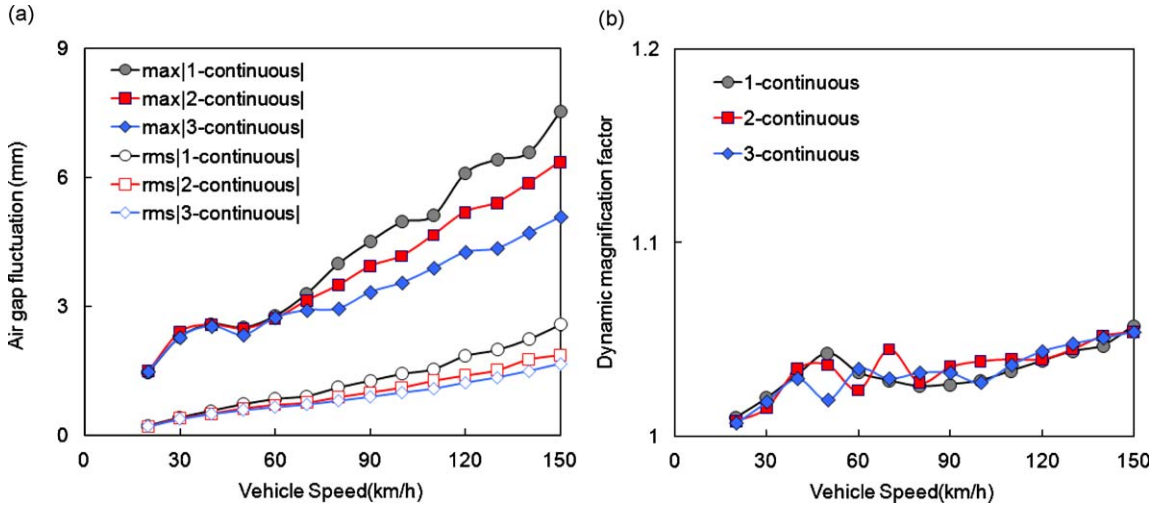

Fig. 10. Effect of span continuity on dynamic responses (deflection ratio = 1500, normal roughness): (a) maximum air gap of maglev vehicle and (b) dynamic magnification factor of guideway girder.

4.6. Damping ratio of guideway structure

Fig. 11 shows the air gap fluctuation of the maglev vehicle and the DMF of the guideway according to various damping ratios of the guideway girder. The damping ratio of the prestressed concrete box beam is generally ranged 0.3–1 percent [27]. It is noticeable that the air gap fluctuation and DMF do not change even when the damping increases up to 10 percent. The reason why the system is insensitive to the inherent structural damping of the guideway girder is explained in the following section specifically.

4.7. Energy of vehicle–guideway interaction system

Fig. 12 shows the energy of the maglev bogies that connect the vehicle cabin and the guideway girder. As can be seen in figure, the total external energy caused by cabin motion, girder deflection, roughness and damper dissipation balances the total internal energy of the maglev bogie. It is clear from the Fig. 12(b) that the input energy from cabin motion are compensated itself by spring and damper of the secondary suspension. Consequently most of input energy originated from the electric current is dissipated by the damper at the secondary suspension.

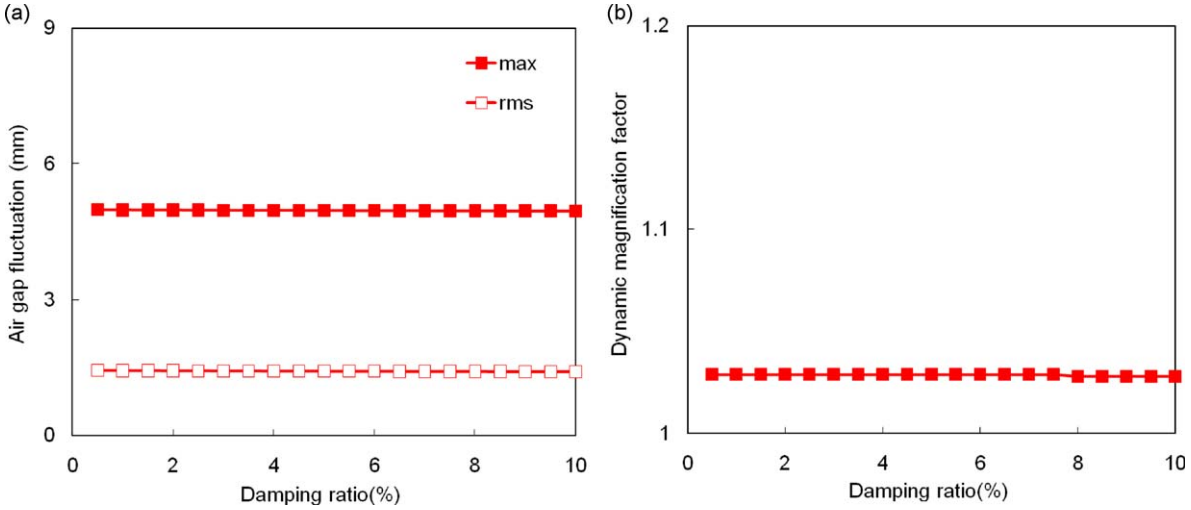

Fig. 11. Effect of inherent damping ratio of guideway on dynamic responses (deflection ratio = 1500, normal roughness, $V = 100$ km/h): (a) maximum air gap fluctuation of maglev vehicle and (b) dynamic magnification factor of guideway girder.

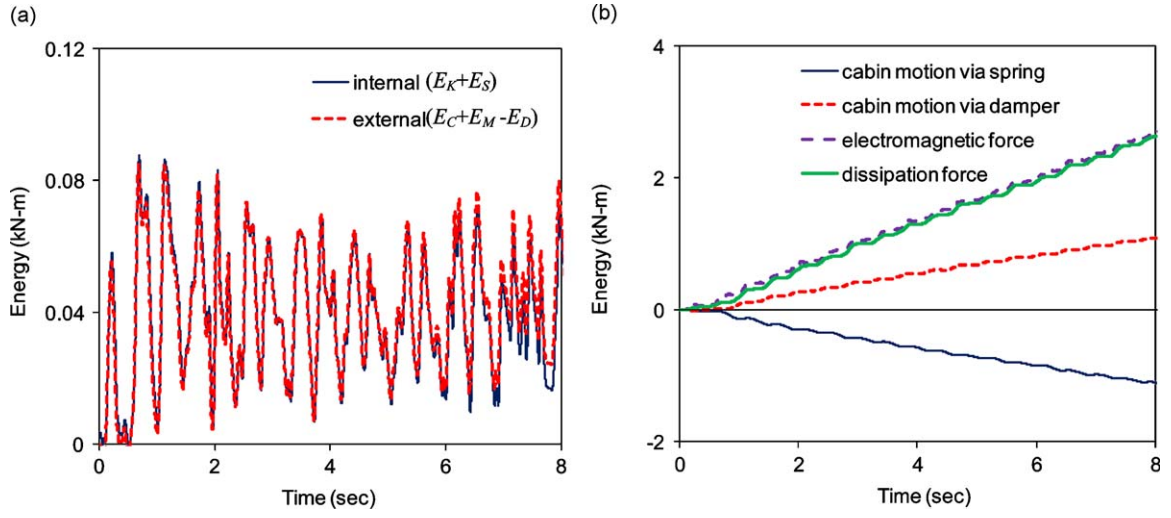

Fig. 12. Energy of the maglev bogie (deflection ratio = 1500, normal roughness, $V = 100$ km/h): (a) balance of internal and external energies and (b) source of external energies.

5. Concluding remarks

In this study, a numerical model is developed for a dynamic interaction analysis of the effects of an actively controlled maglev vehicle and a flexible guideway structure. The effects of various parameters on dynamic responses of the maglev vehicle and guideway structures are then investigated using the developed analysis tool. The maglev vehicle in the present study focuses on the low and medium speed maglev system currently being developed in Korea.

From numerical simulation, it is found that the air gap fluctuation between the magnet and guideway girder linearly increases in proportion to vehicle speed and maximum amplitude of roughness. The air gap fluctuation at a low vehicle speed is governed by surface roughness, yet that at a high vehicle speed is dominated by the deflection of the guideway girder, which is a type of roughness with a very long wavelength. Therefore, a criterion for guideway deflection can be obtained case by case according to the maximum speed of the vehicle. Span continuity also contributes to the change in the air gap. A guideway girder with structurally continuous neighboring spans is effective in attenuating the peak air gap due to the relatively smooth curvature and small deflection slope near the support. However, the effects of span length and damping ratio of the guideway structure on the air gap are insignificant. The overall dynamic magnification factor of the guideway girder is not severe compared with a traditional wheel type vehicle, and is <1.1 for any case in the present low and medium speed maglev system.

Acknowledgments

This work is part of a research project supported by the Korea Ministry of Construction and Transportation (MOCT) through the Korea Railroad Research Institute (KRRI). The authors wish to express their gratitude for the financial support.

Appendix A. The sub-matrices in Eq. (10)

$$\mathbf{A}=\begin{bmatrix}\mathbf{0}_{n\times n} & \mathbf{I}_{n\times n} & \mathbf{0}_{n\times 5} & \mathbf{0}_{n\times 5} & \mathbf{0}_{n\times 3}\\ \mathbf{A}_{21} & \mathbf{A}_{22} & \mathbf{A}_{23} & \mathbf{0}_{n\times 5} & \mathbf{A}_{25}\\ \mathbf{0}_{5\times n} & \mathbf{0}_{n\times n} & \mathbf{I}_{5\times 5} & \mathbf{0}_{5\times 5} & \mathbf{0}_{5\times 3}\\ \mathbf{A}_{41} & \mathbf{A}_{42} & \mathbf{A}_{43} & \mathbf{A}_{44} & \mathbf{A}_{45}\\ \mathbf{0}_{3\times n} & \mathbf{0}_{3\times n} & \mathbf{0}_{3\times 5} & \mathbf{A}_{54} & \mathbf{A}_{55}\end{bmatrix}_{(2n+13)\times(2n+13)} \tag{A.1}$$

$$\mathbf{A}_{21}=\begin{bmatrix}-\omega_1^2 & & 0\\ & \ddots & \\ 0 & & -\omega_n^2\end{bmatrix}_{n\times n} \tag{A.2}$$

$$\mathbf{A}_{22}=\begin{bmatrix}-2\xi_1\omega & & 0\\ & \ddots & \\ 0 & & -2\xi_1\omega_n\end{bmatrix}_{n\times n} \tag{A.3}$$

$$\mathbf{A}_{23}=\begin{bmatrix}0 & 0 & -k_z\phi_1(x_1) & -k_z\phi_1(x_2) & -k_z\phi_1(x_3)\\ \vdots & \vdots & \vdots & \vdots & \vdots\\ 0 & 0 & -k_z\phi_n(x_1) & -k_z\phi_n(x_2) & -k_z\phi_n(x_3)\end{bmatrix}_{n\times 5} \tag{A.4}$$

$$\mathbf{A}_{25}=\begin{bmatrix}k_i\phi_1(x_1) & k_i\phi_1(x_2) & k_i\phi_1(x_3)\\ \vdots & \vdots & \vdots\\ k_i\phi_n(x_1) & k_i\phi_n(x_2) & k_i\phi_n(x_3)\end{bmatrix}_{n\times 3} \tag{A.5}$$

$$\mathbf{A}_{41}=\begin{bmatrix} \sum_{j=1}^{3}\{\phi_1(x_j)+V\phi_1'(x_j)\} & \cdots & \sum_{j=1}^{3}\{\phi_n(x_j)+V\phi_n'(x_j)\} \\ -\sum_{j=1}^{3}a_j\{\phi_1(x_j)+V\phi_1'(x_j)\} & \cdots & -\sum_{j=1}^{3}a_j\{\phi_n(x_j)+V\phi_n'(x_j)\} \\ \left\{\left(\omega_1^2-\frac{k_s}{m_b}\right)\phi_1(x_1)-V\frac{c_s}{m_b}\phi_1'(x_1)-V^2\phi_1''(x_1)\right\} & \cdots & \left\{\left(\omega_n^2-\frac{k_s}{m_b}\right)\phi_n(x_1)-V\frac{c_s}{m_b}\phi_n'(x_1)-V^2\phi_n''(x_1)\right\} \\ \left\{\left(\omega_1^2-\frac{k_s}{m_b}\right)\phi_1(x_2)-V\frac{c_s}{m_b}\phi_1'(x_2)-V^2\phi_1''(x_2)\right\} & \cdots & \left\{\left(\omega_n^2-\frac{k_s}{m_b}\right)\phi_n(x_2)-V\frac{c_s}{m_b}\phi_n'(x_2)-V^2\phi_n''(x_2)\right\} \\ \left\{\left(\omega_1^2-\frac{k_s}{m_b}\right)\phi_1(x_3)-V\frac{c_s}{m_b}\phi_1'(x_3)-V^2\phi_1''(x_3)\right\} & \cdots & \left\{\left(\omega_n^2-\frac{k_s}{m_b}\right)\phi_n(x_3)-V\frac{c_s}{m_b}\phi_n'(x_3)-V^2\phi_n''(x_3)\right\} \end{bmatrix}_{5\times n} \tag{A.6}$$

$$\mathbf{A}_{42}=\begin{bmatrix} \sum_{j=1}^{3}\phi_1(x_j) & \cdots & \sum_{j=1}^{3}\phi_n(x_j) \\ -\sum_{j=1}^{3}a_j\phi_1(x_j) & \cdots & -\sum_{j=1}^{3}a_j\phi_n(x_j) \\ \left\{-\frac{c_s}{m_b}\phi_1(x_1)+2\xi_1\omega_1\phi_1(x_1)-2V\phi_1'(x_1)\right\} & \cdots & \left\{-\frac{c_s}{m_b}\phi_n(x_1)+2\xi_n\omega_n\phi_n(x_1)-2V\phi_n'(x_1)\right\} \\ \left\{-\frac{c_s}{m_b}\phi_1(x_2)+2\xi_1\omega_1\phi_1(x_2)-2V\phi_1'(x_2)\right\} & \cdots & \left\{-\frac{c_s}{m_b}\phi_n(x_2)+2\xi_n\omega_n\phi_n(x_2)-2V\phi_n'(x_2)\right\} \\ \left\{-\frac{c_s}{m_b}\phi_1(x_3)+2\xi_1\omega_1\phi_1(x_3)-2V\phi_1'(x_3)\right\} & \cdots & \left\{-\frac{c_s}{m_b}\phi_n(x_3)+2\xi_n\omega_n\phi_1(x_3)-2V\phi_n'(x_3)\right\} \end{bmatrix}_{5\times n} \tag{A.7}$$

$$\mathbf{A}_{43}=\begin{bmatrix} \mathbf{A}_{431} & \mathbf{A}_{432} \\ \mathbf{A}_{433} & \mathbf{A}_{434} \end{bmatrix}_{5\times 5} \tag{A.8}$$

$$\mathbf{A}_{431}=\begin{bmatrix} \frac{-3k_s}{m_c} & \frac{k_s}{m_c}\sum_{j=1}^{3}a_j \\ \frac{k_s}{I_c}\sum_{j=1}^{3}a_j & \frac{-k_s}{I_c}\sum_{j=1}^{3}a_j^2 \end{bmatrix}_{2\times 2} \tag{A.9}$$

$$\mathbf{A}_{432}=\begin{bmatrix} \frac{k_s}{m_c} & \frac{k_s}{m_c} & \frac{k_s}{m_c} \\ \frac{-a_1k_s}{I_c} & \frac{-a_2k_s}{I_c} & \frac{-a_3k_s}{I_c} \end{bmatrix}_{2\times 3} \tag{A.10}$$

$$\mathbf{A}_{433}=\begin{bmatrix} \frac{k_s}{m_b} & \frac{-a_1k_s}{m_b} \\ \frac{k_s}{m_b} & \frac{-a_2k_s}{m_b} \\ \frac{k_s}{m_b} & \frac{-a_3k_s}{m_b} \end{bmatrix}_{3\times 2} \tag{A.11}$$

$$\mathbf{A}_{434}=\begin{bmatrix} \frac{k_z-k_s}{m_b}+k_z\sum_{l=1}^{n}\left[\phi_l(x_1)\left\{\sum_{j=1}^{3}\phi_l(x_j)\right\}\right] & 0 & 0 \\ 0 & \frac{k_z-k_s}{m_b}+k_z\sum_{l=1}^{n}\left[\phi_l(x_2)\left\{\sum_{j=1}^{3}\phi_l(x_j)\right\}\right] & 0 \\ 0 & 0 & \frac{k_z-k_s}{m_b}+k_z\sum_{l=1}^{n}\left[\phi_l(x_3)\left\{\sum_{j=1}^{3}\phi_l(x_j)\right\}\right] \end{bmatrix}_{3\times 3} \tag{A.12}$$

$$\mathbf{A}_{44}=\begin{bmatrix} \frac{-3c_s}{m_c} & \frac{c_s}{m_c}\sum_{j=1}^{3}a_j & \frac{c_s}{m_c} & \frac{c_s}{m_c} & \frac{c_s}{m_c} \\ \frac{c_s}{I_c}\sum_{j=1}^{3}a_j & \frac{-c_s}{I_c}\sum_{j=1}^{3}a_j^2 & \frac{-a_1c_s}{I_c} & \frac{-a_2c_s}{I_c} & \frac{-a_3c_s}{I_c} \\ \frac{c_s}{m_b} & \frac{-a_1c_s}{m_b} & \frac{-c_s}{m_b} & 0 & 0 \\ \frac{c_s}{m_b} & \frac{-a_2c_s}{m_b} & 0 & \frac{-c_s}{m_b} & 0 \\ \frac{c_s}{m_b} & \frac{-a_3c_s}{m_b} & 0 & 0 & \frac{-c_s}{m_b} \end{bmatrix}_{5\times5} \tag{A.13}$$

$$\mathbf{A}_{45}=\begin{bmatrix} 0 & 0 & 0 \\ 0 & 0 & 0 \\ \frac{-k_i}{m_b}-k_i\sum_{l=1}^{n}\left[\phi_l(x_1)\sum_{j=1}^{3}\phi_l(x_j)\right] & 0 & 0 \\ 0 & \frac{-k_i}{m_b}-k_i\sum_{l=1}^{n}\left[\phi_l(x_2)\sum_{j=1}^{3}\phi_l(x_j)\right] & 0 \\ 0 & 0 & \frac{-k_i}{m_b}-k_i\sum_{l=1}^{n}\left[\phi_l(x_3)\sum_{j=1}^{3}\phi_l(x_j)\right] \end{bmatrix}_{5\times3} \tag{A.14}$$

$$\mathbf{A}_{54}=\begin{bmatrix} 0 & 0 & \frac{k_z}{k_i} & 0 & 0 \\ 0 & 0 & 0 & \frac{k_z}{k_i} & 0 \\ 0 & 0 & 0 & 0 & \frac{k_z}{k_i} \end{bmatrix}_{3\times5} \tag{A.15}$$

$$\mathbf{A}_{55}=\begin{bmatrix} \frac{-R_0}{L_0} & 0 & 0 \\ 0 & \frac{-R_0}{L_0} & 0 \\ 0 & 0 & \frac{-R_0}{L_0} \end{bmatrix}_{3\times3} \tag{A.16}$$

Appendix B. The sub-matrices in Eq. (14)

$$\mathbf{B}=\begin{bmatrix} \mathbf{0}_{(2n+10)\times3} \\ 1/L_0 & 0 & 0 \\ 0 & 1/L_0 & 0 \\ 0 & 0 & 1/L_0 \end{bmatrix}_{(2n+13)\times3} \tag{B.1}$$

$$\mathbf{G}=[3\times13]\text{ state feedback gain} \tag{B.2}$$

$$\mathbf{L}=[13\times6]\text{ observer gain} \tag{B.3}$$

$$\mathbf{C}=\begin{bmatrix} & 0&0&1&0&0&0&0&0&0&0&0&0&0 \\ & 0&0&0&0&0&0&0&1&0&0&0&0&0 \\ \mathbf{0}_{6\times2n} & 0&0&0&1&0&0&0&0&0&0&0&0&0 \\ & 0&0&0&0&0&0&0&0&1&0&0&0&0 \\ & 0&0&0&0&1&0&0&0&0&0&0&0&0 \\ & 0&0&0&0&0&0&0&0&0&1&0&0&0 \end{bmatrix}_{6\times(2n+13)} \tag{B.4}$$

$$\mathbf{f}(t)=[f_{z_{bg1}}\ f_{\dot{z}_{bg1}}\ f_{z_{bg2}}\ f_{\dot{z}_{bg2}}\ f_{z_{bg3}}\ f_{\dot{z}_{bg3}}]^{\mathrm{T}} \tag{B.5}$$

$$\mathbf{H} = \mathbf{I}_{(2n+13)\times(2n+13)} \tag{B.6}$$

$$\mathbf{w}(t) = \left[\mathbf{0}_{1\times n} \quad F_{m0}\sum_{j=1}^{3}\phi_1(x_j) \quad F_{m0}\sum_{j=1}^{3}\phi_2(x_j) \quad \cdots \quad F_{m0}\sum_{j=1}^{3}\phi_n(x_j) \quad \mathbf{0}_{1\times 5} \right.$$
$$\left. \sum_{j=1}^{3}(z_r(x_j)+\dot{z}_r(x_j)) \quad -\sum_{j=1}^{3}a_j(z_r(x_j)+\dot{z}_r(x_j)) \quad F_{b1}(t) \quad F_{b2}(t) \quad F_{b3}(t) \quad \mathbf{0}_{1\times 3} \right]^{\mathrm{T}} \tag{B.7}$$

$$F_{b1}(t) = -\sum_{i=1}^{n}\phi_i(x_1)\left\{\sum_{j=1}^{3}\phi_i(x_j)F_{m0}\right\} - \frac{k_s}{m_b}z_r(x_1) - \frac{c_s}{m_b}\dot{z}_r(x_1) - \ddot{z}_r(x_1) \tag{B.8}$$

$$F_{b2}(t) = -\sum_{i=1}^{n}\phi_i(x_2)\left\{\sum_{j=1}^{3}\phi_i(x_j)F_{m0}\right\} - \frac{k_s}{m_b}z_r(x_2) - \frac{c_s}{m_b}\dot{z}_r(x_2) - \ddot{z}_r(x_2) \tag{B.9}$$

$$F_{b3}(t) = -\sum_{i=1}^{n}\phi_i(x_3)\left\{\sum_{j=1}^{3}\phi_i(x_j)F_{m0}\right\} - \frac{k_s}{m_b}z_r(x_3) - \frac{c_s}{m_b}\dot{z}_r(x_3) - \ddot{z}_r(x_3) \tag{B.10}$$

Appendix C. The energy representations in Eq. (15)

$$E_K = \frac{1}{2}\sum_{j=1}^{3}m_b\dot{z}_{bj}^2 \tag{C.1}$$

$$E_S = \frac{1}{2}\sum_{j=1}^{3}k_s(z_c - z_{bj} - z_{c0})^2 \tag{C.2}$$

$$E_C = \sum_{j=1}^{3}\int_0^t k_s(z_c - z_{bj} - z_{c0})\dot{z}_c\,\mathrm{d}t + \sum_{j=1}^{3}\int_0^t c_s(\dot{z}_c - \dot{z}_{bj})\dot{z}_c\,\mathrm{d}t \tag{C.3}$$

$$E_M = \sum_{j=1}^{3}\int_0^t [-k_i\Delta i + k_z(z_{bj} - z_{gj} - z_r - z_0)]\dot{z}_{bj}\,\mathrm{d}t \tag{C.4}$$

$$E_D = \sum_{j=1}^{3}\int_0^t c_s(\dot{z}_c - \dot{z}_{bj})^2\,\mathrm{d}t \tag{C.5}$$

References

[1] P.K. Sinha, *Electromagnetic Suspension—Dynamics and Control*, IEE, London, 1987.
[2] D.M. Rote, Y. Cai, Review of dynamic stability of repulsive-force maglev suspension systems, *IEEE Transactions on Magnetics* 38 (2) (2002).
[3] R. Thornton, et al., *MagneMotion Urban Maglev*, US DOT, 2004.
[4] S.H. Jung, et al., *Design and Analysis of Bogie Frame of Urban Maglev Vehicle*, ROTEM, 1995 (in Korean).
[5] H.J. Cho, M.H. Yoo, J.M. Lee, *Performance Test and Evaluation of Urban Transit Maglev Vehicle* (*UTM-01*), 1998 (in Korean).
[6] S.H. Han, Y.J. Kim, B.C. Shin, B.H. Kim, Simulation of dynamic interaction between maglev and guideway using FEM, *Maglev2006*, Dresden, 2006.
[7] J.K. Hedrick, R.J. Ravera, J.R. Anderes, The effects of elevated guideway construction tolerances on vehicle ride quality, *Journal of Dynamic Systems, Measurement and Control, ASME* 97 (4) (1975).
[8] Y. Cai, S.S. Chen, S.M. Rote, H.T. Coffey, Vehicle/guideway interaction for high speed vehicles on a flexible guide-way, *Journal of Sound and Vibration* 175 (5) (1994).
[9] S.D. Kwon, J.S. Lee, J.W. Moon, M.Y. Kim, Dynamic interaction analysis of urban maglev vehicle and guideway suspension bridge subjected to gusty wind, *Engineering Structures* 30 (12) (2008).
[10] K. Popp, W. Schiehlen, Dynamics of magnetically levitated vehicles on flexible guideways, *Vehicle System Dynamics* 4 (2) (1975).
[11] D.F. Zhao, W.M. Zhai, Maglev vehicle/guideway vertical random response and ride quality, *Vehicle System Dynamics* 38 (3) (2002).
[12] R. Meisinger, Simulation of a single and double-span guideway under action of moving maglev vehicles with constant force and constant gap, Schriftenreihe der Georg-Simon-Ohm-Fachhochschule Nürnberg Nr.14, Nürnberg, 2002.
[13] N. Hägele, F. Dignath, Vertical dynamics of the maglev vehicle transrapid, *Multibody System Dynamics* 21 (3) (2009).
[14] H. Tsunashima, M. Abe, Static and dynamic performance of permanent magnet suspension for maglev transport vehicle, *Vehicle System Dynamics* 29 (1998).
[15] X.J. Zheng, J.J. Wu, Y.H. Zhou, Numerical analysis on dynamic control of five-degree-of-freedom maglev vehicle moving on flexible guideways, *Journal of Sound and Vibration* 235 (1) (2000).

[16] J. Fang, A. Ardovinsky, D.B. Montgomery, Dynamic modeling and control of the Magplane vehicle, *Maglev2004*, Shanghai, 2004.
[17] M. Morita, M. Iwaya, M. Fujino, The characteristics of the levitation system of Linimo (HSST system), *Maglev2004*, Shanghai, 2004.
[18] V.K. Garg, R.V. Dukkipati, *Dynamics of Railway Vehicle Systems*, Academic Press, New York, 1984.
[19] T.D. Gillespie, *Fundamentals of Vehicle Dynamics*, 1992.
[20] A.E. Bryson, *Applied Linear Optimal Control: Examples and Algorithms*, Cambridge University Press, Cambridge, 2002.
[21] CEMTOOL, Open Lecture for Control System Engineering, 〈http://www.cemtool.co.kr/〉, 2007 (in Korean).
[22] S. Nakamura, *Numerical Analysis and Graphic Visualization with MATLAB*, Prentice-Hall, Englewood Cliffs, NJ, 2002.
[23] T.T. Soong, G.F. Dargush, *Passive Energy Dissipation Systems in Structural Engineering*, Wiley, New York, 1997.
[24] D.A. Hullender, Analytical models for certain guideway irregularities, *Journal of Dynamic Systems, Measurement and Control, ASME* 97 (4) (1975).
[25] H.S. Han, S. Kim, B. Yim, Y. Hur, Stability analysis of a Maglev vehicle utilizing electromagnetic suspension system, *Transactions of Korean Society of Automotive Engineers* 16 (3) (2008) (in Korean).
[26] B.M. Jin, et al., Proposal of maglev guideway girder by structural optimization: civil works of Center for Urban Maglev Program in Korea, *Proceeding of International Conference on Electrical Machines and Systems*, Seoul, 2007.
[27] H. Bachmann, W. Ammann, *Vibrations in Structures*, Structural Engineering Documents 3e, IABSE, 1987.